Probing the Outer Mitochondrial Membrane in Cardiac Mitochondria with Nanoparticles

V. Salnikov,* Y. O. Lukyánenko,† C. A. Frederick,* W. J. Lederer,* and V. Lukyánenko*
*Medical Biotechnology Center, University of Maryland Biotechnology Institute, Baltimore, Maryland 21201; and †Biochemistry and Molecular Biology, University of Maryland School of Medicine, Baltimore, Maryland 21201

ABSTRACT The outer mitochondrial membrane (OMM) is the last barrier between the mitochondrion and the cytoplasm. Breaches of OMM integrity result in the release of cytochrome *c* oxidase, triggering apoptosis. In this study, we used calibrated gold nanoparticles to probe the OMM in rat permeabilized ventricular cells and in isolated cardiac mitochondria under quasi-physiological ionic conditions and during permeability transition. Our experiments showed that under control conditions, the OMM is not permeable to 6-nm particles. However, 3-nm particles could enter the mitochondrial intermembrane space in mitochondria of permeabilized cells and isolated cardiac mitochondria. Known inhibitors of the voltage-dependent anion channel (VDAC), König polyanion, and 4,4′-diisothiocyanatostilbene-2,2′-disulfonic acid inhibited this entrance. Thus, 3-nm particles must have entered the mitochondrial intermembrane space through the VDAC. The permeation of the isolated cardiac mitochondria OMM for 3-nm particles was ~20 times that in permeabilized cells, suggesting low availability of VDAC pores within the cell. Experiments with expressed green fluorescent protein showed the existence of intracellular barriers restricting the VDAC pore availability in vivo. Thus, our data showed that 1), the physical diameter of VDAC pores in cardiac mitochondria is ≥3nm but ≤6 nm, and 2), permeability transition-related mitochondrial swelling results in breaching and disruption of the OMM.

INTRODUCTION

Mitochondria are important intracellular organelles, that when triggered, orchestrate cell death through a cascade of events launched by apoptogenic proteins. An increase in mitochondrial membrane permeability to macromolecules is one of the key events in apoptotic and necrotic death, although the detailed mechanisms remain controversial (1,2).

Recently we described intracellular sarcoplasmic aquatic diffusion pathways (SPADPs) in ventricular cardiomyocytes (3). This work explored how gold nanoparticles could move within a cell and its organelles. Particularly, we showed a difference in the distribution of 3- and 6-nm particles within ventricular cells. The 3-nm particles were localized along the Z-lines and the intermyofibrillar mitochondria and were also seen inside the mitochondria and nucleus, whereas the 6-nm particles were primarily found along the Z-lines but not in the mitochondria or nucleus. Here we continue to study SPADPs in ventricular cells. In our previous study (3) we suggested that 3-nm particles could penetrate the outer mitochondrial membrane (OMM) through the voltage-dependent anion channel (VDAC).

Theoretically, membrane impermeant probes could enter mitochondria through VDACs (4,1), through permeability transition (PT) pores (5–7,2), through mitochondrial apoptosis-related channels (MACs)(8,9), through apoptosis-related ceramide pores (10,11), through protein import channels (translocase outer membrane, TOM), and/or through possible preparative damage to the OMM (12–14,2). Only VDAC and TOM40 are relevant to normal mitochondrial functioning. The four other mechanisms noted above are related to apoptosis and/or PT-related mitochondrial swelling (9,15).

TOM40 is a cation-selective high-conductance channel (16). The effective internal diameter for TOM was probed with preproteins conjugated to gold clusters and determined to be between 2.0 and 2.6 nm (17). These channel characteristics, if correct, exclude the possibility of TOM40 being an entry pathway for nanoparticles ≥3 nm in size. Thus, under quasi-physiological ionic conditions, only VDAC could allow our probes to enter isolated cardiac mitochondria (ICM).

A low-selective VDAC is the only known ionic channel that permits the fast exchange of molecules and ions between extramitochondrial and mitochondrial intermembrane spaces (MIMS) (18–21,7,1,22). Except for a relatively few membrane-permeant lipophilic compounds (e.g., molecular oxygen, acetaldehyde, short chain fatty acids), all metabolites that enter and leave the mitochondria must cross the OMM through the VDAC (22). The protein structure of VDAC have been described in detail for nonmuscle (23,4,20,24) and cardiac cells (25). VDAC is a highly conserved 30–32 kDa protein (26). Each VDAC protein forms a barrel in the bilayer comprised of a transmembrane α-helix and 13 transmembrane β-strands. This β-barrel encloses an aqueous channel of 2–3.2 nm in internal diameter, which in the open state allows passage of nonelectrolytes up to ~5 kDa (27,20,1,28,22).

The size of the VDAC pore is directly connected to the problem of cytochrome *c* release from MIMS. The release of free cytochrome *c* oxidase under some conditions induces

Submitted July 31, 2006, and accepted for publication October 20, 2006.

Address reprint requests to Dr. Valériy Lukyánenko, Medical Biotechnology Center, University of Maryland Biotechnology Institute, 725 W. Lombard St., Rm. S216, Baltimore, MD 21201. Tel.: 410-706-8559; Fax: 410-706-8184; E-mail: lukyanen@umbi.umd.edu.

Vadim Salnikov's permanent address is Kazan Institute of Biochemistry and Biophysics, Kazan Science Center, Russian Academy of Sciences, 2/31 Lobachevskii St., Kazan, Russia 420111.

0006-3495/07/02/1058/14 $2.00

doi: 10.1529/biophysj.106.094318

programmed cell death—apoptosis (29,13,30,14,2). There is also some evidence that VDAC could be involved in the PT pore formation (5–7,2, but see Krauskopf et al. (31)). Meanwhile, both VDAC and PT were shown to be connected to the release of cytochrome *c* initiating apoptosis (13,29,30,32).

It has been suggested that cytochrome *c* could be released from the MIMS via several mechanisms: 1), as result of PT-related swelling, which induces OMM rupture (33,13); 2), through a special channel formed by four VDACs (32); 3), through the MACs (8,9), and/or 4), through ceramide pores (10,11). The ceramides form oligomeric barrel-stave channels with estimated diameters $\geq$10 nm, but only under apoptotic conditions (12,13). To induce the release of macromolecules from the MIMS under normal conditions, ceramides should be added directly to isolated mitochondria (34). The channel activity of MAC correlates with the presence of proapoptotic Bax in the OMM (8). Under normal conditions, Bax predominantly exists as a monomer in the cytosol (35). Dimerization of Bax results in its translocation to the OMM, mitochondrial dysfunction, and apoptosis (35,1). Our experimental conditions excluded translocation of Bax to the OMM and provided us with data in support of PT-related swelling-induced OMM rupture.

Our previous article (3) focused on SPADPs and we only noted that 3- but not 6-nm particles were found in the mitochondria of permeabilized cells. Here we investigate the distribution of these nanoparticles within the mitochondrial borders and in close proximity to the OMM from the cytosolic side and expand the nanoparticle approach to investigate mitochondrial membrane for ''transparency'' to nano-objects. In this article, we present data on the physical clearance of the cardiac VDAC pore under quasi-physiological ionic conditions and suggest a new approach to the study of VDAC pharmacology in vitro.

METHODS

Isolation of heart mitochondria

Hearts from male 300–350 g Sprague-Dawley rats were rapidly removed, chopped, and homogenized in ice-cold isolation buffer containing 225 mM mannitol, 75 mM sucrose, 5 mM Hepes, 1 mM EGTA, and 1 mg/ml bovine serum albumin (BSA) (fatty acid free) with the pH adjusted to 7.4 using KOH. After the first centrifugation (3 min, 600 $\times$ *g*), the supernatant was collected and then centrifuged at 10,000 $\times$ *g* for 10 min. The supernatant and the light fraction of the pellet were discarded. The pellet was resuspended in isolation buffer and centrifuged at 10,000 $\times$ *g* for 10 min. The pellet (mitochondria) was resuspended in 100 μl of isolation buffer without EGTA. The final suspension of the mitochondria (50–60 mg/ml protein assayed by Biuret) was stored on ice and used in experiments within 4 h of preparation.

Isolated cardiac mitochondria (ICM) were placed (5 μl) on a dry coverslip as described previously (36). After 30 s, the unattached mitochondria were washed out with an experimental solution containing 100 mM K^+ aspartate, 20 mM KCl, 3 mM MgATP, 0.81 mM $MgCl_2$ (free $[Mg^{2+}] = \sim$1 mM), 0.1 mM EGTA, 0.03 $CaCl_2$ ($[Ca^{2+}]_{free} = \sim$90 nM), 20 mM Hepes, 10 mM phosphocreatine (disodium salt), 5 U/ml creatine phosphokinase, 3 mM glutamic acid, and 3 mM malic acid, pH 7.2. This is a slightly modified standard solution used to mimic the cardiac cytoplasm content for experiments in permeabilized ventricular cells (37). The free $[Ca^{2+}]_{free}$ and $[Mg^{2+}]_{free}$ at the given total Ca^{2+}, Mg^{2+}, ATP, and EGTA concentrations were calculated using WinMAXC32 2.5 (Stanford University, Stanford, CA). Measurements with a D-Scan spectrofluorometer (PTI, Monmouth Junction, NJ) and the Ca^{2+} indicator fura-2 (TefLabs, Austin, TX) showed that real $[Ca^{2+}]_{free}$ in the experimental solution was $\sim$100 nM.

Unless specified otherwise, all chemicals were from Sigma (St. Louis, MO).

Cell isolation

Single ventricular myocytes were obtained from adult male Sprague-Dawley rat hearts by enzymatic dissociation as described previously (38). Before permeabilization, the cells were kept in the standard Tyrode solution containing (in mM) 140 NaCl, 5.4 KCl, 0.5 $MgCl_2$, 1 $CaCl_2$, 10 Hepes, 0.25 NaH_2PO_4, 5.6 glucose, pH 7.3. Single ventricular myocytes were permeabilized with 0.007% saponin (60 s) as described previously (37). After permeabilization, the cells were exposed to the solution containing 100 mM K^+ aspartate, 20 mM KCl, 3 mM MgATP, 0.81 mM $MgCl_2$ ($[Mg^{2+}]_{free} = \sim$1 mM), 0.5 mM EGTA, 0.114 mM $CaCl_2$ ($[Ca^{2+}]_{free} = \sim$90 nM), 20 mM Hepes, 10 mM phosphocreatine (disodium salt), 5 U/ml creatine phosphokinase, 3 mM glutamic acid, 3 mM malic acid, and 1% polyvinylpyrrolidone (PVP), pH 7.2.

Electron microscopy

The isolated saponin-permeabilized ventricular cells were prepared for electron microscopy (EM) as described previously (3). The preparation included fixation of the cells in 6% glutaraldehyde and embedding in LR White resin (Ted Pella Inc., Redding, CA). For preparation of a monolayer of ICM for the EM, we slightly modified the procedure. Briefly, still attached to coverslips, ICM were fixed in 1% glutaraldehyde and 4% paraformaldehyde in 0.1 M Na-cacodylate buffer (pH 7.4) overnight at 4°C, then rinsed two times with the same buffer supplemented with 0.2 M sucrose and postfixed with 1% osmium in s-Colloidine buffer (Electron Microscopic Science, Hatfield, PA). Then samples were en bloc stained (2% uranyl acetate in 50% ethanol) for 1 h. After dehydration in an alcohol series, the samples were embedded in LR White resin. Ultrathin sections were obtained with an LKB III microtome, (LKB, Bromma, Sweden), collected on Formvar-coated nickel grids, and stained for 15 min with 2% aqueous uranyl acetate followed by lead citrate for 2 min at room temperature. Sections were examined at 60 kV with a Zeiss electron microscope EM 10C/EM 10 CR (Zeiss, Gottingen, Germany). Images were stored in tiff format.

Sometimes mitochondrial granules that are seen with Epon embedding (39,40) were also present on LR White micrographs (3). However, these granules are very rare and much less electron-dense than silver grains. Therefore, they are easily recognized by digitally reducing the contrast of the micrograph.

To probe the physical clearance of the VDAC pore, we used gold nanoparticles (Ted Pella) coated with PVP with minimal sizes of $\sim$3 or 6 nm as was described (3). The original average size of ''5-nm'' gold nanoparticles used in our experiments was 5 $\pm$ 0.75 (mean $\pm$ SD; Ted Pella), whereas for ''2-nm'' colloidal gold only, the range of 1–3 nm is known. Theoretically, the PVP adds $\sim$2 nm to size of the gold core (3) and this final size is important for our experiments. To measure the size of the PVP-coated ''2-nm'' nanoparticles, we employed Dynamic Light Scattering (Protein Solutions, Wyatt Technology, Santa Barbara, CA). The average size of 2-nm gold particles coated with PVP in our experimental solutions was 3.9 $\pm$ 0.51 (mean $\pm$ SD; $n = 10$). However, theoretically the smallest particles in the group must penetrate deeper into the cell or mitochondrion and will be found in larger numbers than particles with the average size. Taking into account the divergence in size (41) and shape (the PVP-coated particles are not perfectly spherical; see Parfenov et al. (3)) within a group, the smallest

PVP-coated particles in a group should be ~1 nm smaller in diameter than the average size. Thus, in our experiments we used two groups of particles with minimal sizes of ~3 or 6 nm. Note also that gold particles with a diameter of <1 nm are unstable and not available as an unconjugated colloidal gold. Thus, the smallest diameter of PVP-coated nanoparticles could not be <3 nm.

Calibrated gold nanoparticles pretreated with 1% PVP were added to ICM or permeabilized ventricular cells after their attachment to coverslips. The density of the nanoparticles in solution was 1.35×10^{14} per ml for 3-nm particles, and 4.5×10^{13} per ml for 6-nm particles. We allowed 20 min for the nanoparticles to diffuse into cells or 10 min to diffuse into ICM and then the ICM or cells were fixed for EM.

To prevent the subsequent movement of nanoparticles inside and outside the mitochondria, we sealed all possible entryways to the mitochondria with glutaraldehyde during fixation (42,43). After preparation for EM, the gold nanoparticles were visualized with silver using the BB International Silver Enhancing Kit (Ted Pella). The size of the silver grains depends on the time of exposure and the accessibility (i.e., depth of position within the section) of the gold. We applied the solution for 8 min. Note because LR White is a water-soluble resin, lipid structures are much ''softer'' after polymerization. This explains the direction of growth of the silver grains around gold cores in the deep of slice toward membranes. To reveal highly electron-dense silver grains, we digitally reduced the image contrast by 70–80% (until only silver particles were clearly seen) with Adobe Photoshop 7.0 (Adobe Systems, San Jose, CA).

Data were expressed as particles/μm^3, taking into account that particles were visualized through the entire thickness of an ultrathin section and assuming the average thickness of the section to be 80 nm. Mitochondrial diameter was measured from round mitochondria or derived from elliptic mitochondria as the square root of the product of maximal and minimal elliptic diameters.

Immunofluorescence

Freshly isolated ventricular cells were fixed in 100% ethanol at -20°C for 1/2 h. They were then washed four times for 15 min with phosphate-buffered saline (PBS), 5% normal goat serum (NGS), 3% BSA. Anti-VDAC (anti-Porin, Ab-5, polyclonal, IgG, Calbiochem, Oncogene Research Product, San Diego, CA) was added at a dilution of 1:50 and incubated overnight at 4°C. As a control, no primary antibody was added to the cells (only PBS, 5% NGS, and 3% BSA). The next day, both control and experimental cells were washed four times for 15 min with PBS, 5% NGS, 3% BSA, second antibody conjugated to Alexa 488 (Molecular Probes, Eugene, OR) was added at a dilution of 1:200, and the cells incubated for 2 h on a rocking platform at room temperature. The cells were then washed four times for 15 min. Slides were made using Slow Fade Light (Molecular Probes) as a mounting medium and stored at −20°C until examined.

Cell transfection

For cell transfection, we used Adenovirus 5, which expresses enhanced green fluorescent protein (GFP; Clontech Laboratories, Mountain View, CA) driven by the cytomegalovirus promoter (AdGFP), which was produced by the Molecular Genetic Core Facility (University of Maryland, Baltimore, MD). Freshly prepared adult rat cardiac myocytes were plated at 50% confluence on laminin-covered coverslips in 35 mm dishes. The plating medium contained: M199 supplemented with 5 mM taurine, 4.4 mM creatine, 2 mM L-carnitine, 3 mM (2-mercaptopropionyl)glycine (i.e., MPG), 19.4 mM glucose, 0.01 U/ml insulin, 0.2% BSA, 50 U/ml penicillin G sodium salt, and 50 μg/ml streptomycin sulfate; 2 h after plating, the bathing solution was replaced with 1 ml of medium containing AdGFP at concentrations 0.6–2.5×10^9 particles/ml. After 90 min, 2 ml of the fresh original medium per dish was added to cells. The cells were used for confocal imaging 2 days after transfection.

Confocal imaging

Prepared slides were examined with a Carl Zeiss Laser Scanning Confocal System (LSM 510, equipped with a C-Apochromat 63 ×/1.2 W corr objective) with excitation at 488 nm and a LP filter 505 nm. All measurements were done from optical slices <1 μm in thickness with a laser beam power of ~0.08 mW.

X-Y scan images were acquired as a mean of 8 and stored in tiff format. Mitochondrial diameters were measured from ~1 μm optical slices using ImageJ 1.31v (National Institutes of Health, Bethesda, MD).

For deconvolution, high resolution *z*-stacks (stacks with a maximum pixel size of 0.1 μm × 0.1 μm × 0.2 μm) were processed using Volocity 3.5.1 (Improvision, Lexington, MA). Images were deconvolved using the iterative restoration algorithm developed by Improvision (Lexington, MA).

Experiments were performed at room temperature (21–23°C). Data were expressed as mean ± SE. Comparisons were made by using the Student's *t*-test, and differences were considered significant when $P < 0.05$.

RESULTS

Immunofluorescence

In isolated cardiac mitochondria, VDAC (also known as porin) was shown to be located in the OMM (44). Fig. 1 shows the distribution of VDAC within rat ventricular myocytes. The immunofluorescence is distributed around the mitochondria. The immunostaining reveals groups of perinuclear and intermyofibrillar (IMFMs) mitochondria, and is clearly

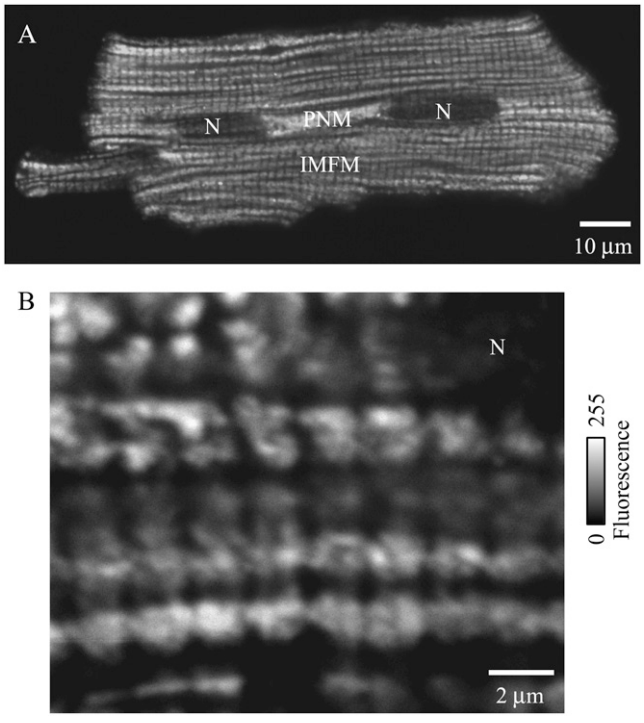

FIGURE 1 Distribution of VDAC in rat ventricular cell. Immunofluorescent labeling. (*A* and *B*) Representative images of cells fixed with ethanol. The cells were incubated overnight with primary antibody. Two cells are shown with lower (*A*) and higher (*B*) resolution. *N*, nucleus; *PNM*, perinuclear mitochondria; and *IMFM*, intermyofibrillar mitochondrion. Optical slice is ~0.7 μm.

absent from Z-lines. Fig. 1 *B* shows IMFM at higher magnification when separate mitochondria can be seen. Similar distribution of VDAC was recorded for 30 other cells.

Permeabilized ventricular cells

Although LR White resin used in our experiments allowed silver ions to penetrate through the thickness of the ultrathin section, the final size of the silver grain was smaller the deeper the gold particle was in the section (see Fig. 2, *circles*). Fig. 2 shows that despite high cytoplasmic density, 6-nm particles did not enter the mitochondria in permeabilized cells. However, some particles were found in close proximity to the OMM on the cytosolic side. Table 1 summarizes all the data pertaining to the density of nanoparticles in our experiments.

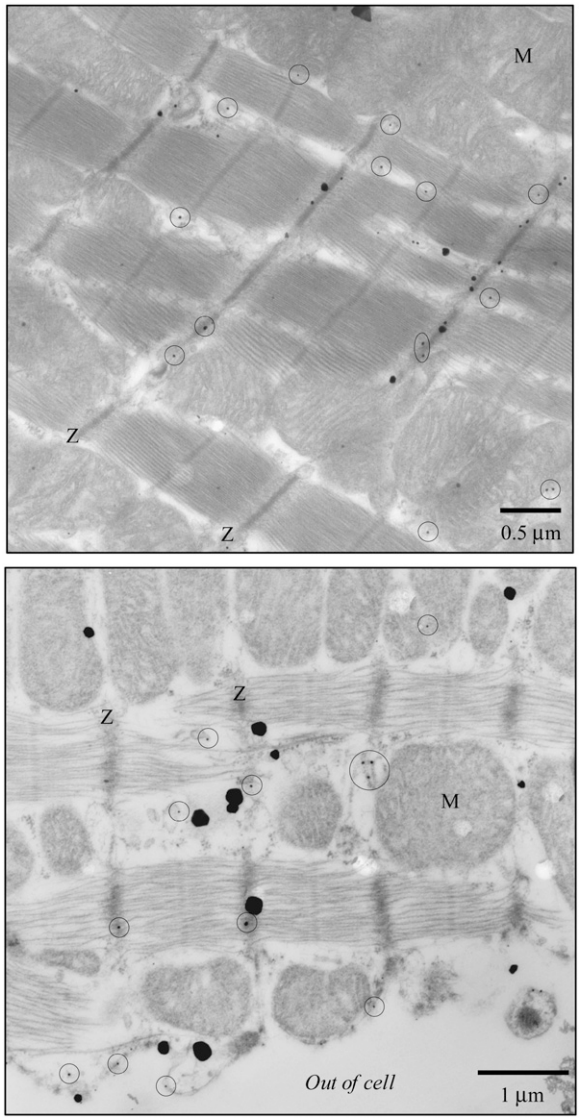

FIGURE 2 Representative electron micrographs made using conventional fixation and silver enhancement show that despite high cytoplasmic density 6-nm particles do not enter mitochondria in permeabilized ventricular myocytes. *M*, mitochondrion; *Z*, Z-line. The solid circles show nanoparticles located deeper inside the ultrathin section and thus have a smaller diameter after silver enhancement.

In contrast to the 6-nm particles, the 3-nm particles entered mitochondria (Fig. 3, *A* and *B*; Table 1). Note that the average density of the 3-nm particles within mitochondria (~8 particles/μm^3) is ~2 times the density of the nanoparticles in the cytosol and ~40 times the density within nucleus under similar ionic conditions (3). In contrast, the density of 6-nm particles was 7 times higher in cytosol (3) than within the mitochondria of permeabilized cells. This indicates that 3-nm particles were trapped within the mitochondria.

If the nanoparticles were entering the mitochondria through the VDAC, inhibition of VDAC should prevent their entering, because in the closed state VDAC is permeable only to small cations (1). Pretreatment of the permeabilized cells with VDAC inhibitors, 15–50 μg/ml König's polyanion (KPA; gift from Dr. Marco Colombini) or 100–300 μM 4,4′-diisothiocyanatostilbene-2,2′-disulfonate (DIDS) (41,42,13, 28), reduced the number of 3-nm particles found in the mitochondria by 80–90% (Fig. 3 *B*; Table 1). This suggests that 3-nm particles entered the MIMS of permeabilized cells through the VDAC.

Isolated cardiac mitochondria, 3-nm particles

The attachment of the ICM to coverslips permitted free gold nanoparticles to wash away from the extramitochondrial space during fixation for EM. Fig. 4 *A* shows the location of 3-nm particles within mitochondria. Note that nanoparticles within the ICM do not show a shape that is specific for PVP-coated granules (3) and tend to aggregate. This suggests that they, at least partially, lost their coating as they entered the ICM. Indeed, neutral PVP should have only a weak tendency to coat gold nanoparticles. Positively charged proteins (such as cytochrome *c* oxidase) within mitochondria should at least partially compete with the effect of gold positive charges. This can result in partial or full ''uncoating'' of the nanoparticles.

Our EM fixation and embedding procedures permitted gold nanoparticles to be marked with silver through the entire volume of the section and reduced the number of ''mitochondrial granules'' (see Parfenov et al. (3)). However, the quality of the imaging would not be as good as would be expected for Epon embedding (45). Therefore, to confirm the location of nanoparticles in the MIMS but not in the mitochondrial matrix, we used a PT inhibitor, cyclosporin (CsA). Fig. 4 *B* shows that pretreatment of the ICM with CsA did not prevent the entry of 3-nm particles (Table 1). Similar to permeabilized ventricular cells, VDAC inhibitors, KPA (15–50 μg/ml), and DIDS (100–300 μM) did significantly inhibited the entering of 3-nm particles by ~80% (Fig. 5, *A* and *B*, correspondingly; Table 1), suggesting that under

TABLE 1 Density of nanoparticles within mitochondria (particles/μm^3) and in close proximity to the OMM (particles/μm)

Group:	Ventricular cells:				ICM:			
Size:	3-nm:		6-nm:		3-nm:		6-nm:	
Position:	Within	OMM	Within	OMM	Within	OMM	Within	OMM
Control	7.6 ± 0.8	~0.02	0.7 ± 0.2‡	~0.08‡	150 ± 14†	~0.04	3.1 ± 1.4†‡	5.6 ± 0.4†‡
n	742		417		114		160	
KPA	0.8 ± 0.5*	~0.01	–	–	26.7 ± 5.7*†	~0.02	–	–
n	104				98			
DIDS	1.4 ± 0.9*	~0.01	–	–	29.7 ± 6.4*†	~0.00	–	–
n	79				88			
High [Ca^{2+}]	–	–	–	–	3.6 ± 1.5*	~0.01	5.0 ± 2.0	4.3 ± 0.3‡
n					104		65	
CATR	–	–	–	–	–	–	26.8 ± 5.0*	1.7 ± 0.1*
n							103	
Alamethicin	–	–	–	–	–	–	14.7 ± 2.6*	0.5 ± 0.1*
n							164	

Mean ± SE. Concentrations used: KPA, 50 μg/ml; DIDS, 300 μM; Ca^{2+}, 150 μM; CATR, 5 μM; alamethicin, 80 μg/ml.
*Data that are statistically different from the corresponding control.
†Data that are statistically different from data for ventricular cells for the same size of nanoparticle.
‡Data that are statistically different from corresponding data for 3-nm particles within the same group ($P < 0.01$); *n*, number of measurements.

control conditions 3-nm particles entered the MIMS through the VDAC.

To increase VDAC gating and consequently restrict the entrance of nanoparticles into ICM ((46), but see Rostovtseva et al. (1)), we supplemented the bathing solution with 150 μM Ca^{2+}. As shown in Fig. 5 *C*, high [Ca^{2+}] resulted in the predictable swelling and changes in mitochondrial ultrastructure (6,12–14,2). Corresponding mean diameters for all experiments with ICM are presented in Table 2. An increase in [Ca^{2+}] in the bathing solution to 150 μM resulted in an ~100% increase in mitochondrial diameter. Although we did not find 3-nm particles within the ICM, they might have been washed out through the membrane openings.

The graph presented in Fig. 5 *D* summarizes the data on densities of 3-nm particles within the ICM. These data assume that the mitochondrial nanogold particles entered ICM through the VDAC, which in this case, must have a pore diameter of ≥3 nm.

Interestingly, if, as it was shown earlier for permeabilized ventricular cells (3), EM fixation and embedding resulted in an ~45% reduction in mitochondrial volume, then under normal conditions the density of 3-nm particles in ICM was ~270 particles/μm^3 before fixation for EM. This is about twice the original density of 3-nm particles in the experimental solution (~120 particles/μm^3). This suggests that 3-nm particles were indeed stuck in the MIMS, which takes up only part of the mitochondrial space. As discussed above, the neutral PVP could be partially stripped from the particles in the middle of ICM due to the competing effects of positively charged proteins. This would result in the particles binding to proteins or in aggregation (3).

Another intriguing observation is that the density of 3-nm particles in ICM under control conditions and after pretreatment with KPA and DIDS was ~20 times higher then in permeabilized ventricular cells (Table 1). This suggests that diffusion of 3 nm particles in permeabilized cells was significantly restricted in comparison to the aqueous solution in our ICM experiments. However, our GFP experiments (see below) showed that diffusion of these size molecules is very fast in permeabilized cells.

Isolated cardiac mitochondria, 6-nm particles

When 6 nm particles were added to ICM under control conditions, they were not found inside the mitochondria (Fig. 6). The density of 6-nm particles within ICM was 50 times less than the density of 3-nm ones (Table 1). Also, unlike the 3-nm particles, 6-nm particles were found primarily in close proximity to the OMM (Table 1; Fig. 6 *B*). If this attachment is similar to the attachment of particles ≥6 nm to glycocalyx as shown in our previous study (3), this would suggest the existence of long chains of glycoproteins on the OMM surface. Such structures can result from damage to the mitochondrial contacts (connecting pillars) to the surrounding intracellular structures (3), mitochondria, and sarcoplasmic reticulum (SR) during their isolation from cardiomyocytes. Indeed, the number of 6-nm particles found on the OMM of ICM was 70 times higher than in permeabilized ventricular myocytes, whereas the density of the nanoparticles within the mitochondria was only 4 times higher in ICM (Table 1). This would suggest that the attachment of 6-nm particles to the OMM might have resulted from the isolation of mitochondria from their natural environment.

Although the diameters of OMM pores may be sufficient to exclude 6-nm particles from entering the MIMS under control conditions, there are two other possible reasons why they did not pass to the geometrical center of the mitochondrion: a), MIMS properties (small distance between cristae

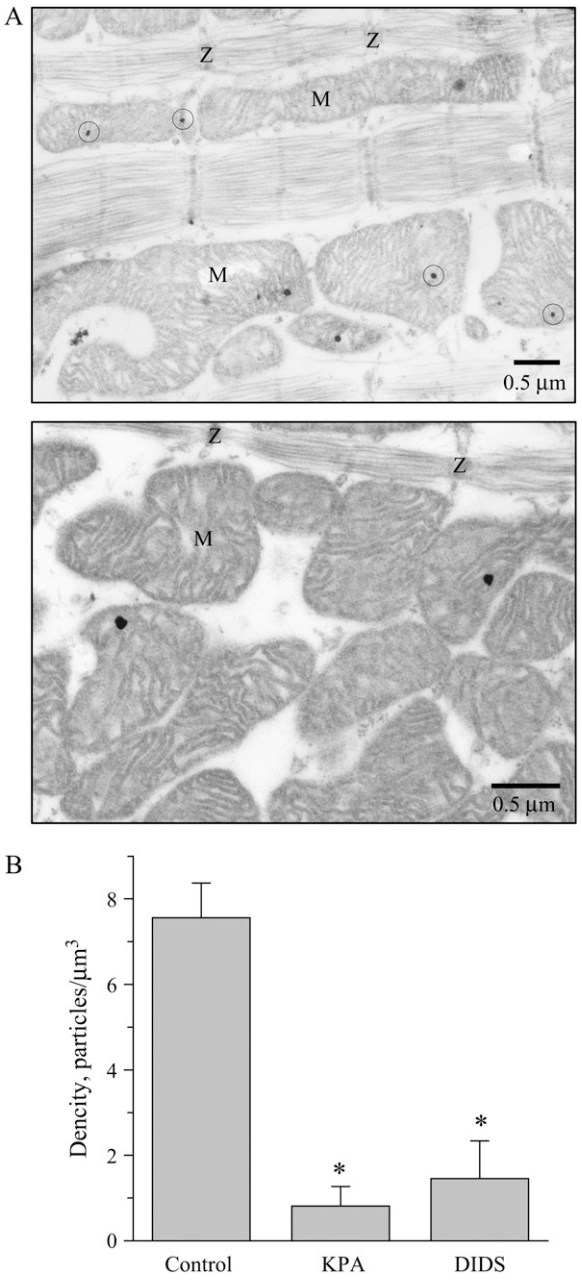

FIGURE 3 Density of 3-nm particles within mitochondria in permeabilized ventricular myocytes. (*A*) Representative electron micrographs made using conventional fixation and silver enhancement show that 3-nm particles enter mitochondria in permeabilized ventricular cells. *M*, mitochondrion; *Z*, Z-line. The solid circles show nanoparticles located deeper inside the ultrathin section and thus have a smaller diameter after silver enhancement. (*B*) The graph shows the load of mitochondria by the particles under marked conditions. Asterisks indicate data that are statistically different from the corresponding control ($P < 0.01$); $n = 79$–742 (see Table 1).

and/or dense content), and/or b), the OMM pillar ''debris'' (left over from the mitochondrial isolation) blocked the entrance. To determine what prevented 6-nm particles from entering the mitochondria, we perforated the mitochondria membranes with 5 μM carboxyatractyloside (CATR) or 80 μg/ml alamethicin. These agents can perforate both the outer and inner mitochondrial membranes but in different ways. CATR binds the C-state of the adenine nucleotide translocator and stimulates the PT pore (6,47,48); whereas alamethicin forms giant pores through both mitochondrial membranes (49,50).

The 10 min pretreatment with CATR resulted in a significant increase in mitochondrial diameters (Table 2) and facilitated the entrance of 6-nm particles into the mitochondria (Fig. 7 *A*). The density of particles within the ICM after 5 μM CATR was ~10 times higher than that under control conditions, whereas attachment of the particles was reduced only 3 times (Table 1).

If 6-nm particles could pass through the PT pore, they should enter the ICM matrix. However, aggregation of the particles within the ICM (Fig. 7 *A*), which is similar to 3-nm particles (Fig. 4), assumes that they entered only the MIMS. Indeed, the simple perforation of both ICM membranes with 80 μg/ml alamethicin also resulted in mitochondrial swelling and a significant increase in the density of intramitochondrial nanoparticles (Tables 1 and 2); however, there was no sign of aggregation of 6-nm particles (Fig. 7 *B*).

Alamethicin forms giant protein pores in both mitochondrial membranes (49,50). Taking into account the original 3 times lower density of 6-nm particles in comparison to 3-nm particles in the experimental solution and the ~4 times alamethicin-induced increase in the volume of the mitochondrial slice (~2 times increase in diameter), the permeation of ICM OMM for 6-nm particles after alamethicin was ~1.5 times higher than for 3 nm particles under control conditions. A very similar increase in density of particles resulted from the effect of CATR (~1.6 times increase). These experiments showed that a), 6-nm particles did not enter the MIMS and bind to the OMM only on the extramitochondrial side; and b), neither the properties of MIMS nor the OMM pillar ''debris'', but the diameter of OMM pores, excludes 6-nm particles from entering the MIMS under normal conditions.

Another way to perforate the OMM in cardiac mitochondria is a Ca^{2+}-induced PT (6,13). Fig. 7 *C* shows the effect of 150 μM Ca^{2+} on OMM permeability. The 6-nm particles were found within ICM in much smaller amounts than after CATR or alamethicin treatment (Table 1), despite a most significant increase in volume (Table 2). The graph presented in Fig. 7 *D* summarizes the data. Visual analysis of ICM ultrathin sections showed that the OMM is severely damaged with high [Ca^{2+}] (see also Brustovetsky et al. (13)). This suggests that 6-nm particles were washed out during EM preparation.

If 6-nm particles enter the ICM after CATR treatment due to multiple membrane breaches resulting from mitochondrial swelling (51,13), this should be seen as a reduction in the number of particles attached to the OMM (the breaches increase the mitochondrial surface area without adding new binding sites for the particles). Therefore, to evaluate the extent of the damage to the OMM induced by the swelling,

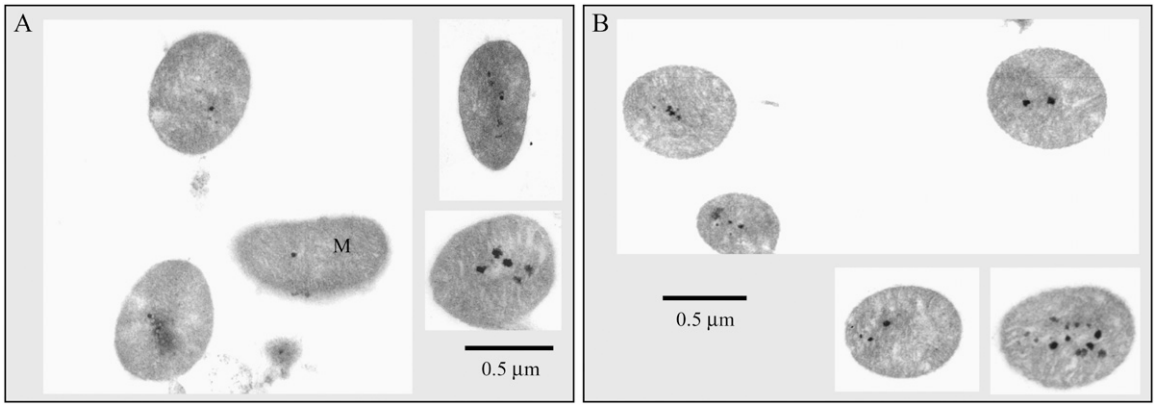

FIGURE 4 Electron micrographs made using conventional fixation and silver enhancement show the location of 3-nm particles in ICM. Representative micrographs show ICM after 10 min of incubation with 3-nm particles in control solution (*A*), and in solution containing 2 μM CsA (*B*). *M*, mitochondrion.

we calculated the number of attached 6-nm particles before and after treatment with CATR or alamethicin. Fig. 8 and Table 1 show that these numbers are significantly reduced by pretreatment with these compounds. Interestingly, high [Ca^{2+}] did not change the number of attached particles suggesting disruption of the OMM.

Distribution of green fluorescent protein in ventricular cell

To determine whether VDAC availability is restricted in intact cells and to evaluate levels of diffusion of 3-nm particles in permeabilized cells, we transfected ventricular cells with GFP ($n = 3$). GFP is a 4.2 nm long cylinder with a cylindrical diameter of only 2.4 nm (52). At pH 7.2, it has a negative charge (–5.6; Protein Calculator v3.3, The Scripps Research Institute, La Jolla, CA). The VDAC could be highly selective to nucleotides (1); however, the shape, size, and negative charge of GFP could allow it to pass through the VDAC of cardiac mitochondria.

We expressed GFP in rat ventricular myocytes and imaged them with confocal microscopy after 48 h. Fig. 9 shows that GFP distributed primarily along the Z-lines and in the nucleus, but not in perinuclear (Fig. 9 *A*, *inset*), subsarcolemmal, or intermyofibrillar (Fig. 9 *C*) mitochondria. Although fluorescence was present in the IMFMs, three-dimensional reconstruction from deconvoluted images showed that it comes from out-of-focus areas and that all three types of cardiac mitochondria are empty of GFP (data not shown).

Could GFP be bound to something located along the Z-lines or does the pattern reflect free distribution of GFP? Fig. 9 *B* shows the same region that was shown in the inset for Fig. 9 *A*, but 1 min after permeabilization. Note that the detection gain was significantly increased to compensate for a decrease in fluorescence due to the leak of GFP from the cell. Permeabilization of the cells with saponin resulted in the release of GFP from all cell compartments excluding nucleus within 1 min ($n = 20$). Previously, we have shown a significant restriction of intracellular aqueous diffusion for particles with size ≥6 nm in permeabilized cells (3). Thus, if GFP was bound to another protein at the Z-line instead of being freely distributed, that protein would have to be much smaller than 2 nm. However, there was the slight possibility of saponin damage to the OMM, which could release GFP. Therefore, to reveal any possible loading of the MIMS with GFP, we reduced the time of exposure to saponin by half (30 s). Membrane blebs filled with GFP confirmed only slight permeabilization (Fig. 9 *E*).

After 30 min, ~50% of the cells showed at least traces of GFP fluorescence (Fig. 9 *E*). However, the GFP diffusion from the nucleus was significantly delayed ($n = 10$). This made the nucleus relatively brighter than the surrounding cytoplasm. If the mitochondria were at least partially loaded with GFP, they should also be seen as relatively brighter structures after release of GFP from the cytoplasm. However, the mitochondria lost their signal proportionally to the background.

All together, the presented GFP data suggest that a), mitochondria of intact cells were not originally filled with GFP (i.e., GFP cannot go through VDAC in its native environment); b), GFP does not bind to sarcoplasmic proteins; c), GFP could diffuse freely within the cell; and d), the space along the Z-lines is opened to free diffusion of particles ~4 nm in size despite the glycogen localized in the same area (40).

DISCUSSION

This is the first investigation, to our knowledge, of permeability of the cardiac OMM pores under quasi-physiological ionic conditions and in their original environment. Under normal conditions only VDAC would allow gold nanoparticles ≥3 nm in size to enter MIMS (see Introduction). In our experiments, the entrance of 3-nm particles into MIMS was significantly restricted in solutions containing KPA and DIDS (Fig. 5 *D*; Table 1), i.e., by two chemical compounds

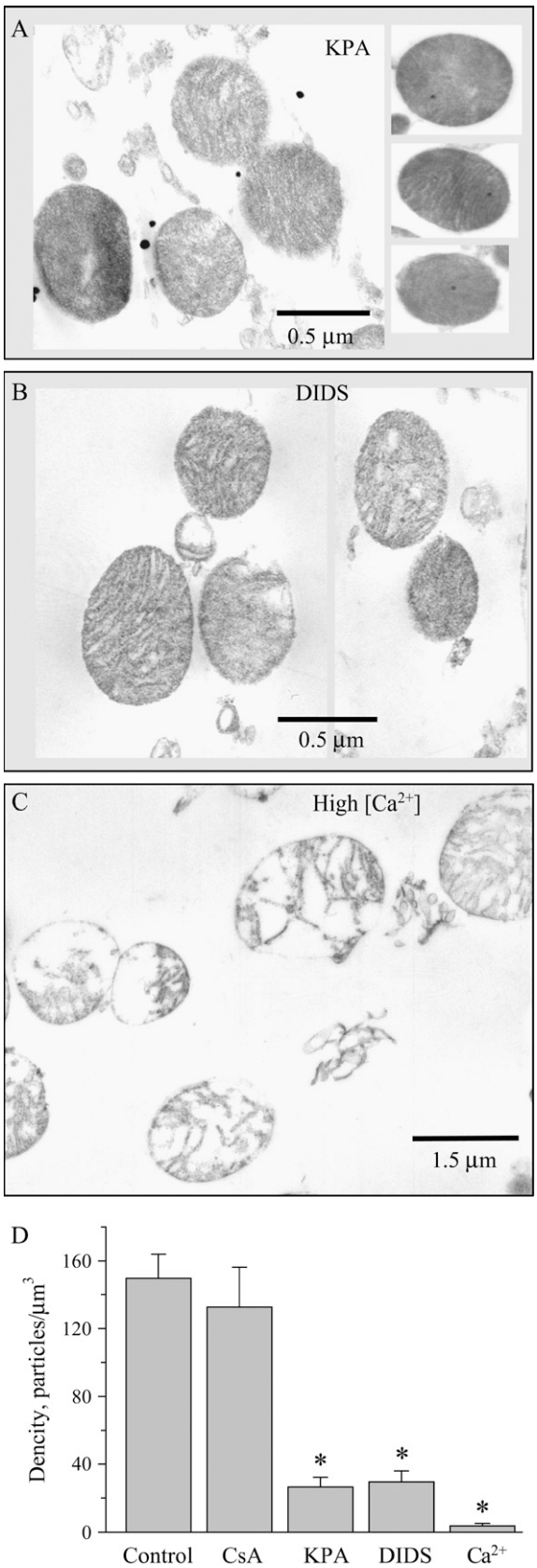

FIGURE 5 Known inhibitors of VDAC prevent entering of 3-nm particles into MIMS. Representative electron micrographs made using conventional fixation and silver enhancement show ICM after 10 min of incubation with 3-nm particles in solutions containing 50 μg/ml KPA (*A*), 300 μM DIDS (*B*), or 150 μM Ca^{2+} (*C*). Nanoparticles were added to the ICM 10 min after the corresponding agent. (*D*) The graph shows the relative load of ICM by the particles under marked conditions ($n = 56$–114). For concentrations used see Table 1. Asterisks indicate data that are statistically different from the corresponding control ($P < 0.01$).

that were shown to be effective inhibitors of VDAC (53, 54,13,28). This suggests that they entered MIMS through the VDAC pore.

Methodology

Theoretically, nanoparticles could enter ICM through VDAC, or through holes in the OMM resulting from mechanical or functional (PT-related) permeabilization of OMM. Under our experimental conditions, the ICM look structurally and functionally undamaged. For instance, Fig. 6 *B* shows fine mitochondrial ultrastructure. In our experimental solution, we used physiological [Mg^{2+}] (~1 mM), which also inhibits PT. This Mg^{2+} effect, however, could be overcome with high [Ca^{2+}] (55). To confirm that our ICM were not initially in the PT state, we performed experiments using CsA, which has been shown to effectively block PT (6). CsA did not change the average number of particles entering mitochondria (Fig. 4 *B*, Table 1). In addition, we confirmed mitochondrial and OMM structural and functional integrity by preventing the filling of MIMS with membrane impermeant fluorescent probes with VDAC inhibitors DIDS and KPA (56), and (2) by loading mitochondrial matrices with fluorescent probes, TMRM, and fluo-3 (AM) (Molecular Probes) in ICM and permeabilized cells (six experiments; not shown). The load with TMRM is a standard test for mitochondrial membrane potential, and the fluo-3 (AM) could produce fluorescence only after deesterification within the mitochondrial matrix.

Our methods also allowed us to discriminate silver grains from ''mitochondrial granules''; however, in our experiments with 3-nm particles (Figs. 4 and 5), the silver grains did not have a typical shape for PVP-coated sols as in the experiments with 6-nm particles under control conditions (Fig. 6 *B*). The 3-nm particles looked aggregated (3). Similar aggregations could also be found within mitochondria when 6-nm particles entered the ICM after CATR (Fig. 7 *A*). This suggests that the PVP coating on the particles was at least partially removed (see Parfenov et al. (3)), possibly by competition from positively charged proteins (as cytochrome *c*), or by positive charges on the inner mitochondrial membrane, which would compete with the positive charge of Au^{3+} located within the gold nanoparticles (57). If this is true, aggregation of particles might be a sign of the matrix's functional and structural integrity. Indeed, when the inner mitochondrial membrane was permeabilized, an even higher concentration

TABLE 2 Diameter (μm) of ICM from ultrathin-section electron micrographs

Control	CsA	KPA	DIDS	High [Ca^{2+}]	CATR	Alamethicin
0.65 ± 0.01	0.62 ± 0.02	0.63 ± 0.04	0.71 ± 0.03	1.24 ± 0.03*	0.91 ± 0.03*†	1.07 ± 0.03*†‡
$n = 396$	122	98	88	169	103	164

Mean ± SE. Concentrations used: CsA, 2 μM; KPA, 50 μg/ml; DIDS, 300 μM; Ca^{2+}, 150 μM; CATR, 5 μM; alamethicin, 80 μg/ml.
*Data that are statistically different from the control.
†Data that are statistically different from data for high [Ca^{2+}].
‡Data that are statistically different from data for CATR ($P < 0.001$); n, number of measurements.

of nanoparticles fails to create such gold aggregations (Fig. 7 *B*).

Another interesting phenomenon is the aggregation of 6-nm particles on the ICM OMM (Fig. 6; Table 1). This is similar to what was found for nonpermeabilized cells, where only particles ≥6 nm attached to the sarcolemma (3). We suggested that this was due to defects in covering of big nanoparticles with PVP, which allowed long branches of glycoproteins to be bound by gold core (41). The OMM bound sites for 6-nm particles could result from the disruption during preparation of ICM of multiple connecting pillars between mitochondria and the surrounding structures shown for cardiac cells (3). Indeed, in permeabilized cells, the number of 6-nm particles located in close proximity to the OMM was considerably less in comparison to ICM (Table 1).

Size of the VDAC pore

The VDAC was shown to be a convergence point for various signaling pathways leading to the cell death, and all of them are mediated with the release of cytochrome *c* oxidase from MIMS (2). Under normal conditions, positively charged cytochrome *c* (the smallest side of cytochrome *c* is ~3 nm; see Margoliash (58)) stays in the MIMS (1). Thus, VDAC's pore opening cannot be much bigger then 3 nm. Our experiments showed that uncharged particles ≥3 nm but not ≥6 nm could enter MIMS. This is in good agreement with previous data by Mannella's group, which showed that the diameter of the open VDAC pore to be ~3 nm (4). However, our measurements are in disagreement with those made with polyethylene glycols by Carneiro et al. (27). They showed that the VDAC's pore is asymmetric, and in the open state had a minimum diameter of ~2 nm. Despite a slight diversity in size, the nanoparticles we designated ''3-nm'' could not have particles with diameter ≤2 nm. Gold particles with diameter of ≤1 nm are unstable and not available as a unconjugated colloidal gold (Ted Pella). In addition, PVP 10000 adds ~2 nm to the diameter of gold particle (3) assuming tight packing on the particle surface. However, even if the original size of the gold particle was less than 1 nm theoretically, it would lead to less compact packing of the PVP and should add more than 2 nm to diameter of the particles. Therefore, we could conclude that our particles could not be less then 3 nm in size and that the VDAC pore diameter is ≥3 nm. The disagreement with measurements made with polyethylene glycols (27) could be explained by changes in polyethylene glycol shape within the pore toward increase in size.

Our data were supported indirectly by experiments with PVP-coated nanoparticles and ferritin loaded into cells. In 1962, C. M. Feldherr showed that after cell injection, gold nanoparticles ~5 nm in size did not enter the MIMS (59), whereas ferritin was localized between the outer and inner mitochondrial membranes (60). A similar distribution of ferritin could be seen in liver cells (61) and skinned skeletal fibers (42). Thus, ferritin passed through the VDAC pore into MIMS and its smallest size should be smaller then the pore. The diameter of the ferritin molecule iron core is ~2.0 nm

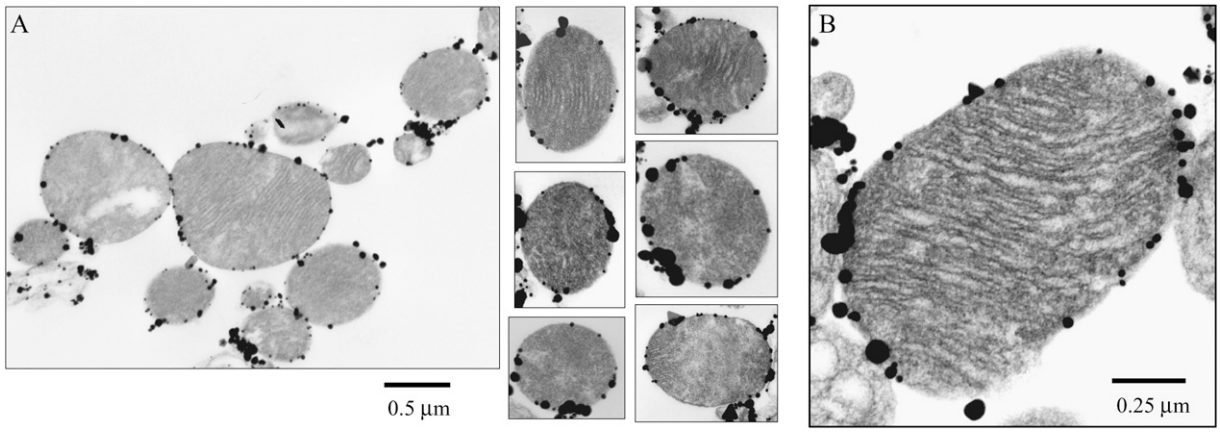

FIGURE 6 Electron micrographs made using conventional fixation and silver enhancement show that 6-nm particles do not enter ICM. Representative micrographs show ICM after 10 min preincubation in the control solution under lower (*A*) and higher (*B*) resolution.

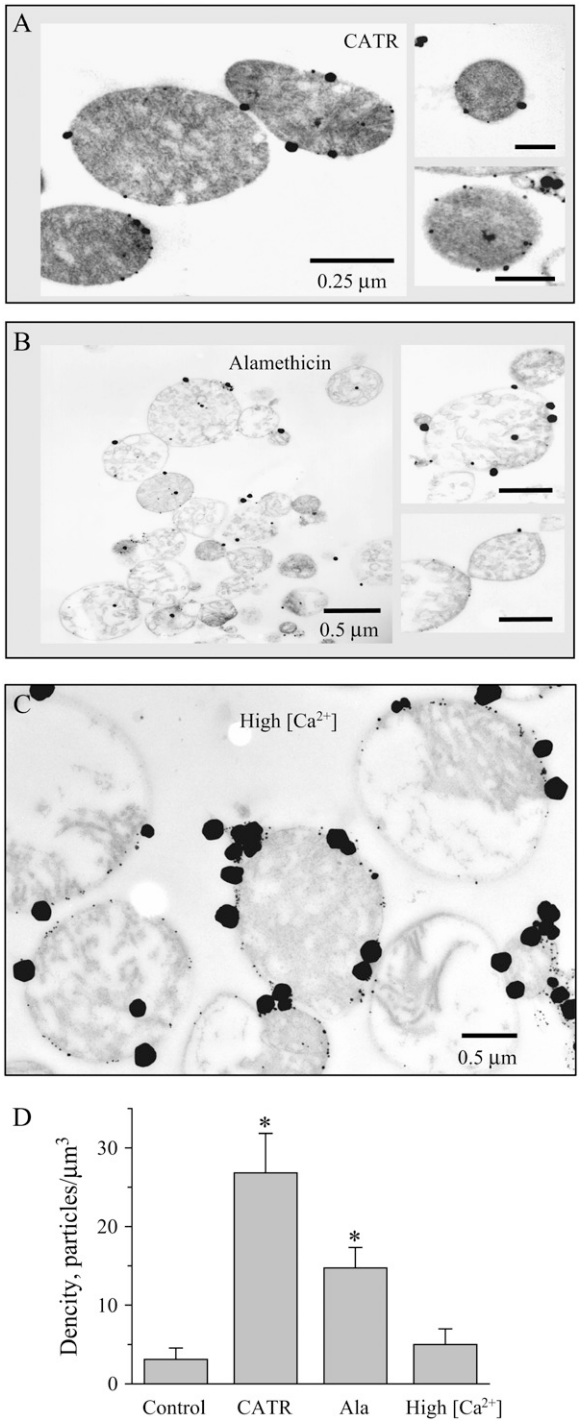

FIGURE 7 Pore formation allows 6-nm particles to enter the MIMS. Representative electron micrographs made using conventional fixation and silver enhancement show ICM after 10 min preincubation in solutions containing 5 μM CATR (*A*), 80 μg/ml alamethicin (*B*), or 150 μM Ca^{2+} (*C*). Nanoparticles were added to the ICM 10 min after pore former. (*A*) All bars, 0.25 μm. (*B*) All bars, 0.5 μm. (*D*) The graph shows the load of ICM by the particles under marked conditions. Asterisks indicate data that are statistically different from the corresponding control ($P < 0.01$); $n = 65$–164 (see Table 1).

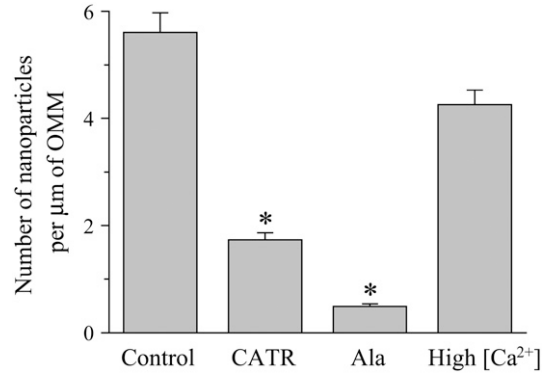

FIGURE 8 Pore formation reduces the number of nanoparticles attached to OMM. The graph shows the number of particles attached to OMM of ICM for control conditions and after preincubation of ICM with 5 μM CATR, 80 μg/ml alamethicin (*Ala*), or 150 μM Ca^{2+} (see Fig. 7). Asterisks indicate data that are statistically different from the corresponding control ($P < 0.01$); $n = 65$–164 (see Table 1).

(61). However, the real diameter is bigger due to a dextran shell, which should add at least 1 nm to the diameter of ferritin iron core (61). This in agreement with our conclusion that the size of VDAC pore is $\geq$3 nm.

PT pore in ICM

In many cells, programmed cell death, apoptosis, is triggered by the release of apoptogenic proteins from the MIMS, of which cytochrome *c* oxidase is the major player (14). Once released, this protein activates a cascade of events leading to apoptotic or necrotic death (14,2). The role of the PT in these processes remains controversial (14,2). Our experiments with 6-nm particles, CATR, and high [Ca^{2+}] helps to clarify the possible mechanisms of PT-related release of cytochrome *c* oxidase. Cytochrome *c* was shown be released from MIMS as a result of PT-related swelling followed by the OMM rupture (12–14), through the VDAC's tetramers (32), and/or through the 4-nm MAC (8,9). However, the channel activity of MAC depends on the presence of proapoptotic Bax in the OMM. Prevention of Bax translocation from the cytoplasm to the OMM prevents formation of MAC and apoptosis (8). CATR induced the entrance of 6-nm particles through the OMM, which could not be through MAC since these experiments were nominally Bax-free. If CATR did not induce mitochondrial synthesis of ceramides (that has not been shown so far) and the opening of 10 nm pores in the OMM (11), only a modified or reorganized VDAC and/or swelling-induced OMM damage could be involved in the penetration of 6-nm particles under our experimental conditions.

In our experiments, CATR significantly changed the diameter of the mitochondria (Table 2). Although the ICM after CATR had much poorer structural integrity than under control conditions, the damage was not as great as after alamethicin treatment (Fig. 7 *B*) or high [Ca^{2+}] (Fig. 7 *C*), and the aggregation of nanoparticles in the middle of the

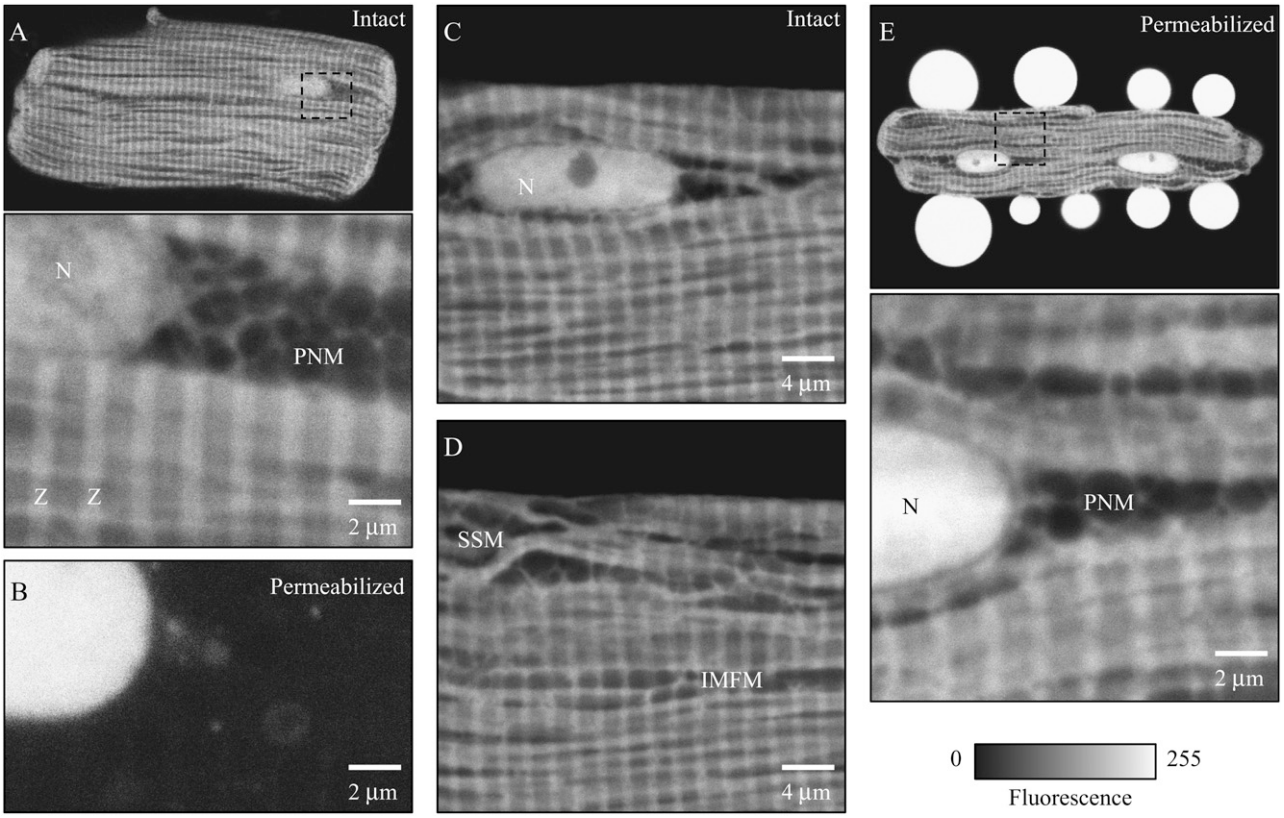

FIGURE 9 Distribution of GFP in rat ventricular myocytes 48 h after adenoviral transfection. GFP fluorescence visualizes intracellular aqueous diffusion pathways. Representative *x-y* images of intact (from two cells, *A, C*, and *D*) ventricular cells, and the cells after saponin permeabilization (*B* and *E*) show the absence of GFP in major groups of mitochondria: perinuclear, subsarcolemmal, and intermyofibrillar. (*A* and *E*) Lower panels represent images of areas marked with dotted square on upper images but with higher magnification. (*B*) 1 min permeabilization. Detection gain was increased 1.35 times to compensate for the decrease in fluorescence due to leak of GFP. All other images were recorded and presented using the same recording and presenting parameters. Therefore, the difference in fluorescence represents the difference in GFP production by the cells. (*E*) 30 s permeabilization. Multiple GFP-filled blebs indicate gentle permeabilization. *N*, nucleus; *SSM*, subsarcolemmal; *PNM*, perinuclear; and *IMFM*, intermyofibrillar mitochondrion. $[Ca^{2+}] = 90$ nM.

mitochondrion (Fig. 7 *A*) also suggests that they retained functional integrity. However, taking into account the ~3 times lower original density of 6-nm particles in the experimental solution and the ~3 times increase in volume, the permeation of the ICM OMM after CATR for 6-nm particles was ~1.5 times higher than the permeation for the 3-nm particles under control conditions through VDAC. This means that the number of available pores for 6 nm particles after CATR was about twice what it was for 3-nm particles under control conditions. If the 6 nm particles entered the MIMS because the VDACs were reorganized into tetramers (32), then we would expect to see a fourfold reduction in mitochondrial density of nanoparticles as compared to the 3 nm particles. Instead we recorded ~100% increase in permeability. Thus, they could not enter MIMS through VDACs reorganized into tetramers, and VDAC tetramers are unlikely to be the pathway for cytochrome *c* oxidase to leave MIMS during mitochondrial swelling.

Thus, CATR-induced increase in OMM permeation could have resulted only from swelling-related OMM damage (51,13). This was also confirmed by the significant reduction in the number of 6-nm particles attached externally to the OMM after CATR treatment (Table 1). The density of attached particles even after correction for changes in ICM diameters (Table 2) was ~2 times less than under control conditions. Curiously, this number almost matched the 1.5× increase discussed above in the number of 6-nm particles within ICM.

Thus, we suggest that under our experimental conditions, PT resulted in damage to the OMM, creating breaches in the membrane. These PT-related openings in OMM, as measured with nanoparticles, would be big enough to release cytochrome *c* oxidase from MIMS and are not the result of reorganized VDACs.

Availability of VDAC for 3-nm particles in vivo

In our previous article (3), we showed that connecting pillars seen between IMFM and junctional SR (jSR) are not fixation artifacts but really exist in vivo. As a result, the jSR is so close to IMFM that gaps between them are not available even for 3-nm particles.

Our current experiments with 6-nm particles indirectly confirmed the existence of such tight contacts between mitochondria and surrounding cell structures. In the nanoparticles, only the gold core is ''sticky'' because it has positive charges. Coating the gold particles ≥6 nm with PVP prevents the aggregation of the particles, but does not prevent their nonspecific binding to the glycocalyx of intact ventricular cells (3). This could be explained by the existence of unevenness in the PVP-coating of particles ≥6 nm, which made the positive charged gold available to long branches of glycoproteins. We have to suggest the same for the ICM; however, the existence of such proteins on outer side of the OMM has not been shown yet. The connecting pillars that are seen very well on EM micrographs of intact ventricular cells (see Parfenov et al. (3)) are assumed to be disrupted during the ICM preparation. Thus, only the existence of their remains on the OMM outer surface could reasonably explain the attachment of 6-nm particles. Indeed, Table 1 shows that the attachment of 6-nm particles to ICM OMM is 70 times the attachment to OMM of mitochondria in permeabilized cells.

Comparison of data from permeabilized ventricular cells and ICM also shows a significant difference in the permeation of OMM (Table 1); 3-nm particles are found in 20 times greater amounts in ICM than in permeabilized ventricular cells. This could result from OMM damage during isolation of the cardiac mitochondria. However, blocking the entrance of 3-nm nanoparticles with VDAC inhibitors assumes that ICM OMM was not damaged. If this is the case, then VDAC inhibitors would have no effect on the entrance of 3-nm nanoparticles, which is what we found. There are only two possible explanations for seeing less 3 nm particles in permeabilized cells: first, diffusion of 3 nm particles in permeabilized cells was very slow so that under our conditions there was not enough time for more particles to enter; or second, VDAC is almost unavailable, either by restricted access or some other factor, for 3 nm particles in vivo. The diffusion limitation for ADP in close proximity to mitochondria was shown recently in saponin-permeabilized heart bundles (62). However, our experiments with GFP confirmed that fast diffusion of molecules as big as the nanoparticles used here was possible, when permeabilization is really complete (Fig. 9). We used similar permeabilization for delivery of nanoparticles into ventricular cells. Thus, the first possibility does not seem reasonable. The second explanation is more likely given the fact that mitochondria have multiple structural connections with the network SR. Earlier we have shown that these can block the entrance for 3-nm particles to the cleft between IMFM and jSR (3). Another explanation is that the VDAC pore entrance in vivo could be covered by huge hexokinases II (12,63,7,1), which could be lost during the preparation of ICM.

The hypothesis that the VDAC pore availability is restricted in their real environment was confirmed in our experiments with GFP. Although the size and charge of GFP should allow it to pass through the VDAC (1), we did not find it within the mitochondria of intact transfected ventricular cells (Fig. 9) as would be expected if the VDACs were available.

The expressed GFP was found primarily along Z-lines and within nuclei. This is in agreement with our data described earlier for the distribution of 3- and 6-nm particles in permeabilized ventricular cells (3). Interestingly, permeabilization of the cell with saponin released the GFP much faster from the myofilament zone than from the nucleus (Fig. 9, *A* and *B*). Comparison of our data with data from Bustamante et al. ((64); they used FITC-labeled dendrimers of 5.4 nm) suggests that particles ~5.5 nm can freely diffuse through cardiac nuclear pores. Thus, contrary to zones along the Z-line, GFP could adhere to nuclear structures, slowing down the saponin-stimulated release.

CONCLUSIONS

The presented data allowed us to conclude that:

1. 3-nm particles enter the MIMS through VDAC.
2. The physical diameter of the VDAC pore is ≥3 nm but ≤6 nm.
3. PT damages the OMM and opens it for particles ≥6 nm in size.
4. Ca^{2+} overload of ICM induces mitochondrial swelling and disruption of the OMM.
5. The OMM has multiple connectors to surrounding intracellular structures.
6. The VDAC pore and MIMS are unreachable in vivo for particles ≤3-nm in size.

We thank Dr. Christos Chinopoulos (Dept. of Anesthesiology, School of Medicine, University of Maryland, Baltimore, MD) for providing us with the isolated cardiac mitochondria and consultation. Also, we thank Drs. Tatiana K. Rostovtseva (Laboratory of Physical and Structural Biology, National Institute of Child Health and Human Development, National Institutes of Health, Bethesda, MD) and Leonyd Breydo (Medical Biotechnology Center, University of Maryland Biotechnology Institute, Baltimore, MD) for reading this manuscript and valuable comments.

This work was supported by grants from the National Institutes of Health (HL36974, HL70709, HL67849, and HL25675).

REFERENCES

1. Rostovtseva, T. K., W. Tan, and M. Colombini. 2005. On the role of VDAC in apoptosis: fact and fiction. *J. Bioenerg. Biomembr.* 37: 129–142.
2. Tsujimoto, Y., T. Nakagawa, and S. Shimizu. 2006. Mitochondrial membrane permeability transition and cell death. *Biochim. Biophys. Acta.* 1757:1297–1300.
3. Parfenov, A. S., V. Salnikov, W. J. Lederer, and V. Lukyanenko. 2006. Aqueous diffusion pathways as a part of the ventricular cell ultrastructure. *Biophys. J.* 90:1107–1119.
4. Mannella, C. A. 1998. Conformational changes in the mitochondrial channel protein, VDAC, and their functional implications. *J. Struct. Biol.* 121:207–218.

5. Zoratti, M., and I. Szabo. 1995. The mitochondrial permeability transition. *Biochim. Biophys. Acta.* 1241:139–176.
6. Crompton, M. 1999. The mitochondrial permeability transition pore and its role in cell death. *Biochem. J.* 341:233–249.
7. Vyssokikh, M., and D. Brdiczka. 2004. VDAC and peripheral channeling complexes in health and disease. *Mol. Cell. Biochem.* 256: 117–126.
8. Pavlov, E. V., M. Priault, D. Pietkiewicz, E. H. Cheng, B. Antonsson, S. Manon, S. J. Korsmeyer, C. A. Mannella, and K. W. Kinnally. 2001. A novel, high conductance channel of mitochondria linked to apoptosis in mammalian cells and Bax expression in yeast. *J. Cell Biol.* 155: 725–731.
9. Guo, L., D. Pietkiewicz, E. V. Pavlov, S. M. Grigoriev, J. J. Kasianowicz, L. M. Dejean, S. J. Korsmeyer, B. Antonsson, and K. W. Kinnally. 2004. Effects of cytochrome *c* on the mitochondrial apoptosis-induced channel MAC. *Am. J. Physiol. Cell Physiol.* 286: C1109–C1117.
10. Siskind, L. J., A. Davoody, N. Lewin, S. Marshall, and M. Colombini. 2003. Enlargement and contracture of C2-ceramide channels. *Biophys. J.* 85:1560–1575.
11. Siskind, L. J., R. N. Kolesnick, and M. Colombini. 2006. Ceramide forms channels in mitochondrial outer membranes at physiologically relevant concentrations. *Mitochondrion.* 6:118–125.
12. Zamzami, N., and G. Kroemer. 2001. The mitochondrion in apoptosis: how Pandora's box opens. *Nat. Rev. Mol. Cell Biol.* 2:67–71.
13. Brustovetsky, N., T. Brustovetsky, R. Jemmerson, and J. M. Dubinsky. 2002. Calcium-induced cytochrome *c* release from CNS mitochondria is associated with the permeability transition and rupture of the outer membrane. *J. Neurochem.* 80:207–218.
14. Halestrap, A. 2005. A pore way to die. *Nature.* 434:578–579.
15. Mannella, C. A. 2006. The relevance of mitochondrial membrane topology to mitochondrial function. *Biochim. Biophys. Acta.* 1762: 140–147.
16. Hill, K., K. Model, M. T. Ryan, K. Dietmeier, F. Martin, R. Wagner, and N. Pfanner. 1998. Tom40 forms the hydrophilic channel of the mitochondrial import pore for preproteins. *Nature.* 395:516–521.
17. Schwartz, M. P., and A. Matouschek. 1999. The dimensions of the protein import channels in the outer and inner mitochondrial membranes. *Proc. Natl. Acad. Sci. USA.* 96:13086–13090.
18. Schein, S. J., M. Colombini, and A. Finkelstein. 1976. Reconstitution in planar lipid bilayers of a voltage-dependent anion-selective channel obtained from Paramecium mitochondria. *J. Membr. Biol.* 30:99–120.
19. Colombini, M., C. L. Yeung, J. Tung, and T. König. 1987. The mitochondrial outer membrane channel, VDAC, is regulated by a synthetic polyanion. *Biochim. Biophys. Acta.* 905:279–286.
20. Colombini, M. 2004. VDAC: the channel at the interface between mitochondria and the cytosol. *Mol. Cell. Biochem.* 256/257:107–115.
21. Mannella, C. A. 1992. The 'ins' and 'outs' of mitochondrial membrane channels. *Trends Biochem. Sci.* 17:315–320.
22. Lemasters, J. J., and E. Holmuhamedov. 2006. Voltage-dependent anion channel (VDAC) as mitochondrial governator. Thinking outside the box. *Biochim. Biophys. Acta.* 1762:181–190.
23. Guo, X. W., P. R. Smith, B. Cognon, D. D'Arcangelis, E. Dolginova, and C. A. Mannella. 1995. Molecular design of the voltage-dependent, anion-selective channel in the mitochondrial outer membrane. *J. Struct. Biol.* 114:41–59.
24. Yehezkel, G., N. Hadad, H. Zaid, S. Sivan, and V. Shoshan-Barmatz. 2006. Nucleotide-binding sites in the voltage-dependent anion channel: characterization and localization. *J. Biol. Chem.* 281:5938–5946.
25. Anflous, K., O. Blondel, A. Bernard, M. Khrestchatisky, and R. Ventura-Clapier. 1998. Characterization of rat porin isoforms: cloning of a cardiac type-3 variant encoding an additional methionine at its putative N-terminal region. *Biochim. Biophys. Acta.* 1399:47–50.
26. Komarov, A. G., D. Deng, W. J. Craigen, and M. Colombini. 2005. New insights into the mechanism of permeation through large channels. *Biophys. J.* 89:3950–3959.
27. Carneiro, C. M., P. G. Merzlyak, L. N. Yuldasheva, L. G. Silva, F. P. Thinnes, and O. V. Krasilnikov. 2003. Probing the volume changes during voltage gating of Porin 31BM channel with nonelectrolyte polymers. *Biochim. Biophys. Acta.* 1612:144–153.
28. Shoshan-Barmatz, V., and A. Israelson. 2005. The voltage-dependent anion channel in endoplasmic/sarcoplasmic reticulum: characterization, modulation and possible function. *J. Membr. Biol.* 204:57–66.
29. Madesh, M., and G. Hajnoczky. 2001. VDAC-dependent permeabilization of the outer mitochondrial membrane by superoxide induces rapid and massive cytochrome *c* release. *J. Cell Biol.* 155:1003–1015.
30. Borutaite, V., A. Jekabsone, R. Morkuniene, and G. C. Brown. 2003. Inhibition of mitochondrial permeability transition prevents mitochondrial dysfunction, cytochrome *c* release and apoptosis induced by heart ischemia. *J. Mol. Cell. Cardiol.* 35:357–366.
31. Krauskopf, A., O. Eriksson, W. J. Craigen, M. A. Forte, and P. Bernardi. 2006. Properties of the permeability transition in VDAC1−/− mitochondria. *Biochim. Biophys. Acta.* 1757:590–605.
32. Zalk, R., A. Israelson, E. S. Garty, H. Azoulay-Zohar, and V. Shoshan-Barmatz. 2005. Oligomeric states of the voltage-dependent anion channel and cytochrome *c* release from mitochondria. *Biochem. J.* 386: 73–83.
33. Brenner, C., and G. Kroemer. 2000. Apoptosis. Mitochondria–the death signal integrators. *Science.* 289:1150–1151.
34. Elrick, M. J., S. Fluss, and M. Colombini. 2006. Sphingosine, a product of ceramide hydrolysis, influences the formation of ceramide channels. *Biophys. J.* 91:1749–1756.
35. Gross, A., J. Jockel, M. C. Wei, and S. J. Korsmeyer. 1998. Enforced dimerization of BAX results in its translocation, mitochondrial dysfunction and apoptosis. *EMBO J.* 17:3878–3885.
36. Vergun, O., T. V. Votyakova, and I. J. Reynolds. 2003. Spontaneous changes in mitochondrial membrane potential in single isolated brain mitochondria. *Biophys. J.* 85:3358–3366.
37. Lukyanenko, V., and S. Györke. 1999. Ca^{2+} sparks and Ca^{2+} waves in saponin-permeabilized cardiac myocytes. *J. Physiol.* 521:575–585.
38. DuBell, W. H., W. J. Lederer, and T. B. Rogers. 2000. K^+ currents responsible for repolarization in mouse ventricle and their modulation by FK-506 and rapamycin. *Am. J. Physiol. Heart Circ. Physiol.* 278: H886–H897.
39. Peachey, L. D. 1964. Electron Microscopic observations on the accumulation of divalent cations in intramitochondrial granules. *J. Cell Biol.* 20:95–111.
40. Fawcett, D. W., and N. S. McNutt. 1969. The ultrastructure of the cat myocardium. I. Ventricular papillary muscle. *J. Cell Biol.* 42:1–45.
41. De Roe, C., P. J. Courtoy, and P. Baudhuin. 1987. A model of protein-colloidal gold interactions. *J. Histochem. Cytochem.* 35:1191–1198.
42. Franzini-Armstrong, C. 1971. Studies of the triad. II. Penetration of tracers into the junctional gap. *J. Cell Biol.* 49:196–203.
43. Hayat, M. A. 1986. Glutaraldehyde: role in electron microscopy. *Micron and Microscopica Acta.* 17:115–135.
44. Konstantinova, S. A., C. A. Mannella, V. P. Skulachev, and D. B. Zorov. 1995. Immunoelectron microscopic study of the distribution of porin on outer membranes of rat heart mitochondria. *J. Bioenerg. Biomembr.* 27:93–99.
45. Maunsbach, A. B., and B. A. Afzelius. 1999. Biomedical Electron Microscopy. Academic Press, New York.
46. Bathori, G., and G. Hajnóczky. 2005. Control of the permeability properties of isolated outer mitochondrial membranes and purified VDAC by Ca^{2+}. *Biophys. J.* 88:2174. (Abstr.)
47. Gincel, D., H. Zaid, and V. Shoshan-Barmatz. 2001. Calcium binding and translocation by the voltage-dependent anion channel: a possible regulatory mechanism in mitochondrial function. *Biochem. J.* 358: 147–155.
48. Gizatullina, Z. Z., Y. Chen, S. Zierz, and F. N. Gellerich. 2005. Effects of extramitochondrial ADP on permeability transition of mouse liver mitochondria. *Biochim. Biophys. Acta.* 1706:98–104.

49. Gostimskaya, I. S., V. G. Grivennikova, T. V. Zharova, L. E. Bakeeva, and A. D. Vinogradov. 2003. In situ assay of the intramitochondrial enzymes: use of alamethicin for permeabilization of mitochondria. *Anal. Biochem.* 313:46–52.

50. Bechinger, B. 1999. The structure, dynamics and orientation of antimicrobial peptides in membranes by multidimensional solid-state NMR spectroscopy. *Biochim. Biophys. Acta.* 1462:157–183.

51. Blondin, G. A., and D. E. Green. 1967. The mechanism of mitochondrial swelling. *Proc. Natl. Acad. Sci. USA.* 58:612–619.

52. Yang, F., L. G. Moss, and G. N. Phillips, Jr. 1996. The molecular structure of green fluorescent protein. *Nat. Biotechnol.* 14:1246–1251.

53. König, T., B. Kocsis, L. Meszaros, K. Nahm, S. Zoltan, and I. Horvath. 1977. Interaction of a synthetic polyanion with rat liver mitochondria. *Biochim. Biophys. Acta.* 462:380–389.

54. Bathori, G., I. Szabo, I. Schmehl, F. Tombola, A. Messina, V. De Pinto, and M. Zoratti. 1998. Novel aspects of the electrophysiology of mitochondrial porin. *Biochem. Biophys. Res. Commun.* 243:258–263.

55. Szabo, I., P. Bernardi, and M. Zoratti. 1992. Modulation of the mitochondrial megachannel by divalent cations and protons. *J. Biol. Chem.* 267:2940–2946.

56. Chinopoulos, C., W. J. Lederer, G. Fiskum, and V. Lukyanenko. 2004. The Ca^{2+} cycling in isolated rat cardiac mitochondria. *Biophys. J.* 86: 108a. (Abstr.)

57. Sau, T. K., A. Pal, N. R. Jana, Z. L. Wang, and T. Pal. 2001. Size controlled synthesis of gold nanoparticles using photochemically prepared seed particles. *J. Nanoparticle Res.* 3:257–261.

58. Margoliash, E. 1963. Primary structure and evolution of cytochrome C. *Proc. Natl. Acad. Sci. USA.* 50:672–679.

59. Feldherr, C. M., and J. M. Marshall. 1962. The use of colloidal gold for studies of intracellular exchanges in the ameba Chaos chaos. *J. Cell Biol.* 12:640–645.

60. Feldherr, C. M. 1962. The intracellular distribution of ferritin following microinjection. *J. Cell Biol.* 12:159–167.

61. Richter, G. W. 1959. The cellular transformation of injected colloidal iron complexes into ferritin and hemosiderin in experimental animals; a study with the aid of electron microscopy. *J. Exp. Med.* 109:197–216.

62. Kongas, O., M. J. Wagner, F. ter Veld, K. Nicolay, J. H. van Beek, and K. Krab. 2004. The mitochondrial outer membrane is not a major diffusion barrier for ADP in mouse heart skinned fibre bundles. *Pflugers Arch.* 447:840–844.

63. Pastorino, J. G., and J. B. Hoek. 2003. Hexokinase II: the integration of energy metabolism and control of apoptosis. *Curr. Med. Chem.* 10: 1535–1551.

64. Bustamante, J. O., E. R. Michelette, J. P. Geibel, J. A. Hanover, T. J. McDonnell, and D. A. Dean. 2000. Dendrimer-assisted patch-clamp sizing of nuclear pores. *Pflugers Arch.* 439:829–837.